Antiresonant Guiding Optofluidic Biosensor

Edward P. Furlani1,[1*], Roshni Biswas,[2] Alexander N. Cartwright,[1,2] and Natalia M. Litchinitser[2]

[1]*The Institute for Lasers, Photonics and Biophotonics, University at Buffalo, Buffalo, NY,14260, USA*
[2]*Electrical Engineering Department, University at Buffalo,Buffalo, NY, 14260, USA*
efurlani@buffalo.edu

Abstract: We propose a novel optofluidic biosensor in which detection is based on a shift in the transmission spectrum due to the contrast in refractive index between the carrier fluid and the target biomaterial. The sensor can function using focused illumination without the need for fiber or waveguide coupled input/output signals. We study the spectral response of the sensor using 2D full-wave time-harmonic field analysis and perform parametric analysis of detection sensitivity as a function of material and device parameters. Our analysis demonstrates that detectible shifts in the transmission spectrum can be achieved with nanoscale accumulation of biomaterial within the sensor. We show that the transmission minima and detection sensitivity can be estimated using analytical expressions based on a 1D antiresonant waveguide model.

Keywords: optofluidic biosensor, photonic bandgap biosensor, microstructure optical fiber, ARROW waveguide biosensor.

1. Introduction

The interest in compact, portable and inexpensive biosensors has grown dramatically in recent years due in part to advances in microfluidics, especially lab-on-a-chip technology. A relatively new and promising approach to biosensing involves optofluidics where optic and fluidic functionality are integrated into a microsystem to leverage their combined advantages [1,2]. Microfluidic functionality enables compact and rapid processing of small biofluid samples, and optical functionality enables high detection sensitivity of target biomaterials within these samples. To date, various optofluidic sensing devices have been developed. Many of these utilize a detection scheme based on some form of resonant optical behavior with input/output signals carried by optical fibers or integrated waveguides that are oriented parallel to the plane of detection. Examples of these include waveguide coupled photonic crystal resonators and Whispering Gallery Mode (WGM)-based sensors [3-7]. While such sensors are capable of high detection sensitivity, they have potential drawbacks both in terms of input/output coupling efficiency and the ease of multiplexing, i.e. addressing multiple independent sensing stations on a single platform. Specifically, the in-plane orientation of the input/output waveguides makes it difficult to realize a two-dimensional array of independent sensing stations on a single platform. Two-dimensional multiplexed sensing is desirable for high-throughput screening of a specimen, which may need to be screened for a large number of different pathogens. In this paper we address this need by proposing and designing a novel, compact optofluidic biosensor that is based on an antiresonant optical waveguide (ARROW)-like structure [8-14]. We theoretically design and numerically characterize the performance of the proposed device and demonstrate the performance that is comparable of exceeding that of a number of proposed sensor technologies [15,16] with a significant advantage of the ease of multiplexing and of light in- and out-coupling.

2. Sensor Operation

The proposed sensor operates in a transmission mode using focused incident illumination wherein the input/output signals propagate perpendicular to the plane of detection thereby eliminating the need for in-plane fiber or waveguide coupled signals. A sensing element consists of multiple parallel microchannels embedded in a substrate and oriented perpendicular to its surface as shown in Fig. 1. The central microchannel is illuminated by a focused beam of light. The periodic spacing of the channels and contrast in refractive index between the carrier fluid and the substrate act to confine and guide the incident light through the central channel similar to that of an antiresonant reflecting optical waveguide (ARROW) [8-12]. Note that the widths of the low-index (fluidic) channels in our design are chosen to be equal to the core width. This is to make the entire structure "transparent" in a direction perpendicular to light propagation direction at the wavelength corresponding to the resonances of high-index layers as discussed below [9]. The transmission spectrum of the sensor is obtained using a detector positioned beneath the central microchannel. The transmission is a function of the wavelength of the incident light, the dimensions, periodicity and refractive index of the substrate, and the refractive index of the carrier fluid. Sensing is achieved via accumulation of a thin (nanoscale) layer of target biomaterial on the surface of the microchannels, which are functionalized (e.g. using immobilized capture antibodies) to bind with the biomaterial as it flows through the system. **Numerous methods have been developed for immobilizing capture antibodies on substrates for microfluidic biosensing applications as described in reference [17]**. The detection in this sensor is based on a shift in the transmission spectrum caused by the contrast in refractive index between the carrier fluid and the target biomaterial.

The transverse nature of the illumination and detection makes the sensing element suitable for multiplexing wherein a single sensor would consist of a two-dimensional array of such elements, each functionalized with a different capture agent to enable simultaneous screening of a specimen for the presence of a large number of different pathogens. The focused input illumination for multiplexed operation could potentially be achieved using a microlens array, or alternatively a multiplexed superluminescent source that is raster scanned across the sensor. The detection could potentially be addressed using a recently reported integrated CMOS color detector [18].

3. Sensor Simulation and Performance

In order to determine the performance of the sensor, we study its electromagnetic response using two different numerical methods: finite element analysis (FEA) and the Beam Propagation Method. These methods have been implemented in commercial software programs and we use the COMSOL RF solver (www.comsol.com) and the Rsoft software (www.rsoftdesign.com) for these methods, respectively. We use these methods to study the transmission spectrum of the sensor at optical wavelengths as a function of the width (thickness) and refractive index of the

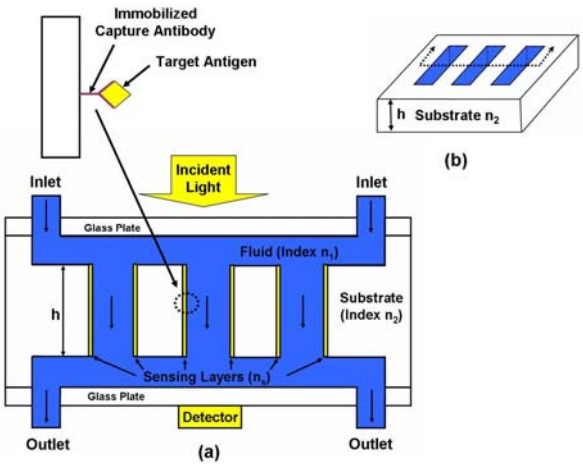

Fig. 1. Sensing element of a microfluidic biosensor: (a) cross-section of microsystem showing microchannels with functionalized sensing layers, (b) perspective view of substrate.

sensing layer. Our analysis demonstrates that a detectable shift in the transmission spectrum can be achieved with nanoscale layers of biomaterial and with little contrast in refractive index between the biomaterial and carrier fluid. We further show that the transmission minima and detection sensitivity can be estimated using analytical expressions that are based on an ARROW model. The proposed sensor is suitable for two-dimensional multiplexed sensing and holds substantial potential for numerous biosensing applications.

We study the spectral response of a sensing element using FEA-based 2D full-wave time-harmonic field analysis. It suffices to study a reduced computational domain with the top and bottom glass cover plates removed as shown in Fig. 2. It is important to note that we obtained substantially the same spectral response with and without the cover plates. For the numerical analysis, we apply perfectly matched layers (PMLs) at the top and bottom of the computational domain to reduce backscatter from these boundaries (Fig. 2). Similarly, scattering boundary conditions are imposed at the boundaries transverse to the direction of propagation to reduce backscatter from these boundaries as well. The central microchannel is illuminated with a downward directed Gaussian-like beam. The incident field is generated by a time-harmonic surface current positioned immediately below the upper PML. The magnitude of the surface current has a Gaussian spatial profile and the direction of the current is into and out of the page, which is taken to be along the z-axis as indicated in Fig. 2.

For the initial analysis we choose a sensing element with three identical microchannels etched through a substrate. The microchannels are chosen to be 4 μm wide and separated from one another by 4 μm wide substrate layers. Thus, the channels are spaced 8 μm centre-to-center. Fluid inlet and outlet channels, above and below the substrate respectively, are taken to be 12 μm in height, i.e. the upper and lower PML layers are 12 μm above and below the substrate, respectively. The fluid and substrate have a refractive index of $n_1 = 1.33$ (H_2O) and $n_2 = 1.45$ (SiO_2), respectively. We compute the time-averaged power P_{in} through the top and P_{out} through the bottom of the central microchannel at optical wavelengths. We take the ratio of these values to determine the transmission $T(h, \lambda, w_s, n_s)$ through the channel,

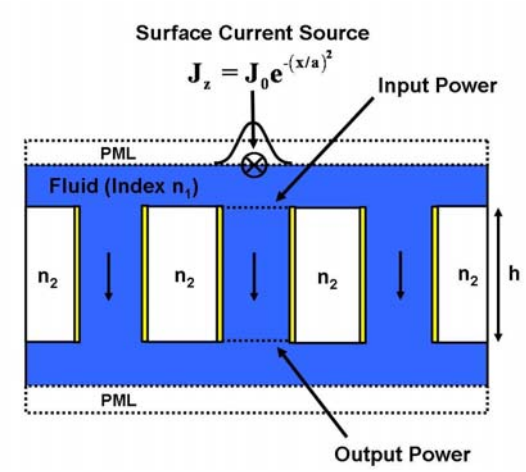

Fig. 2. Computational model for a sensing element.

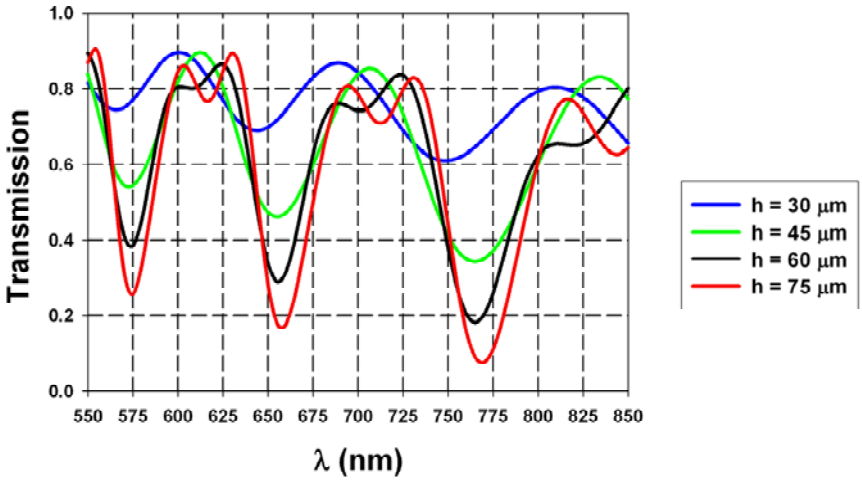

Fig. 3. Transmission vs. wavelength as a function of substrate thickness *h*.

$$T(h,\lambda,w_s,n_s)=\frac{P_{out}(h,\lambda,w_s,n_s)}{P_{in}(h,\lambda,w_s,n_s)}. \qquad (1)$$

Significantly, the transmission depends on several variables including the height h of the microchannels, the wavelength λ of the incident light and the width w_s and refractive index n_s of the sensing layer.

We first compute the transmission spectrum as a function of the channel height *h* (Fig. 2). These results are in excellent agreement with those obtained by a complimentary RSoft Beam Propagation Method. For this analysis there are no sensing layers. A time-harmonic surface

current with a Gaussian spatial profile $J_z = J_0 \exp\left(-\left(x/a\right)^2\right)$ (A/m) (a = 2 μm) is applied below the upper PML. We compute the spectral response for a range of wavelengths λ = 550-850 nm and for four different channel heights h = 30, 45, 60 and 75 μm as shown in Fig. 3. The computational domain for this analysis consisted of 202,496 cubic elements and it took less than 40 minutes to compute each transmission spectrum using a dual quad-core workstation with 24 GB of RAM. From Fig. 3 we find that the transmission spectrum exhibits more clearly defined and pronounced minima as the thickness (h) of the substrate increases. This is expected because as h increases the structure more closely resembles a planar ARROW structure, which has very narrow minima [9]. However, there is a practical limit to the depth of the microchannel relative to its width, i.e. the aspect ratio is limited by microfabrication processes and substrate material properties. For the remaining analysis we use an aspect ratio of 15:1, and thus for 4 μm microchannels we set h = 60 μm. While this ratio might be challenging to obtain using a SiO_2 substrate, it can be achieved using low-loss materials such as SU8 ($n_2 \approx$ 1.6-1.8).

The spectral response of the sensing element can be understood by recognizing that its optical configuration is similar to a planar ARROW [8-12]. Light launched down the low-index central microchannel will be partially guided via antiresonant reflections from the lateral high- and low-index layers formed by the high refractive index substrate and low refractive index carrier fluid, respectively. As such, the transmission minima can be estimated using a simple analytical expression. The transmission minima for a planar ARROW structure occur at [8,9]

$$\lambda_m = \frac{2n_1 d}{m}\left[\left(\frac{n_2}{n_1}\right)^2 - 1\right]^{\frac{1}{2}} \quad (m = 1, 2, \ldots) \qquad (2)$$

where n_1 is the index of the low-index (carrier fluid) layer and d and n_2 are the width and index of the high-index (substrate) layer. It should be noted that Eq. (2) applies when $\lambda / w_c << 1$, where w_c is the width of the central microchannel. This condition is approximately satisfied for this sensor (w_c = 4 μm, λ = 550-850 nm). From Eq. (2) we find that over the range of wavelengths studied, transmission minima occur at λ_6 = 770 nm, λ_7 = 660 nm and λ_8 = 578 nm respectively. These estimates are in close agreement with numerically computed minima shown in Fig. 3 for h = 60 and 75 μm. Thus Eq. (2) can be used to estimate the performance of the sensing element. More importantly, the existence of multiple transmission minima enable enhanced detection accuracy as described below.

Next, we perform a parametric analysis to determine the spectral response of the sensor as a function of the refractive index of the sensing layer n_s = 1.33, 1.35,…, 1.45, (i.e. $n_1 \leq n_s \leq n_2$). The width of the sensing layer is fixed, w_s = 100 nm. We also fix h = 60 μm as above and compute the transmission spectra as shown in Fig. 4a. Note that the transmission minima shift toward longer wavelengths as n_s increases. As shown in Figure 4b the transmission minima at λ_6 = 770 nm exhibit a nearly linear shift of approximately $\Delta\lambda$ = 10 nm towards longer wavelengths for every change in refractive index of $\Delta n = n_s - n_1 = 0.03$ between the sensing layer and carrier fluid. Thus, a refractive index change of 1 will produce a shift of 333 nm, which corresponds to a sensitivity of ~333 nm/RIU, which makes it competitive with comparable sensors that are based on 2-D photonic crystals, planar ring resonators, and microsphere ring resonators [15] While further design optimization and advancements in fabrication of high aspect ratio waveguiding structures would be required for the ARROW-based technique to meet higher sensitivity standards set by plasmon resonance based technologies, the biosensor proposed here has significant advantages, which include the ease of multiplexing and coupling of light into the sensor. An additional feature of this sensor is that multiple relatively closely spaced transmission minima at different wavelengths can be used for detection. This enables enhanced detection accuracy.

A number of previously published refractometric sensor designs have been characterized using a figure of merit (FOM) that is defined as the ratio of sensitivity to the full width at half maximum of the transmission minimum [19]. For example, a recent comparative study of refractometric sensors based on propagating versus localized surface plasmons demonstrate a FOM~50 for both approaches. Using the above definition, we estimate the FOM for our device to be ~60.

Another important feature of the sensor is that the detection sensitivity can be tuned by choosing appropriate substrate dimensions, layer widths and refractive indices. Significantly, the width and index of the sensing layer (w_s and n_s) can be controlled by labeling the target biomaterial with a dielectric nanoparticle of a given diameter D_p and refractive index n_p. The size of the nanoparticle determines the width of the sensing layer ($w_s \cong D_p$), and maximum sensitivity can be achieved by choosing $n_p = n_2$. When this is the case, the shift in the

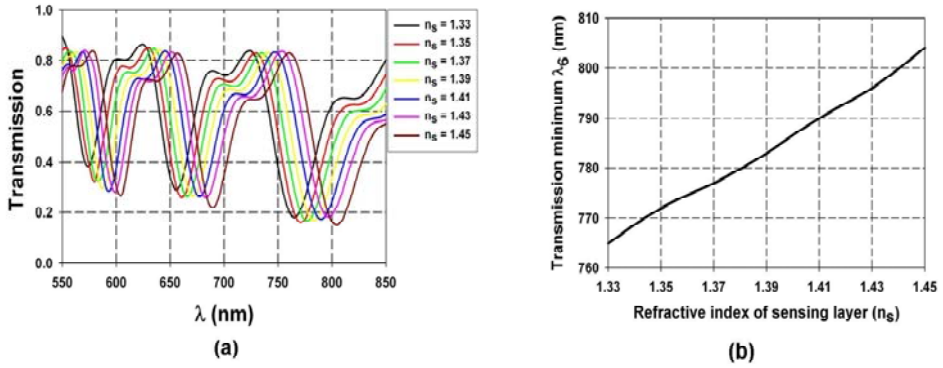

Fig. 4. Transmission spectra: (a) spectra for different n_s, (b) transmission minimum wavelength λ_6 vs. n_s.

transmission spectrum can be estimated using Eq. (2), i.e

$$\Delta\lambda_m = \frac{2n_1\Delta d}{m}\left[\left(\frac{n_2}{n_1}\right)^2 - 1\right]^{\frac{1}{2}} \quad (m = 1, 2, \ldots) \tag{3}$$

where $\Delta\lambda_m$ is the shift in the m'th minima and $\Delta d = 2w_s$ is the effective change in width of the substrate layer. To demonstrate this principle, consider the shift in λ_6 i.e. the m = 6 minimum of the transmission spectrum. We use Eq. (3) to estimate the spectral sensitivity at this minimum, i.e. the shift in λ_6 as a function the width of the sensing layer w_s when $n_s = n_2$. The shift is linear with respect to w_s, i.e. $\Delta\lambda_6 = \frac{4w_s}{6}\sqrt{\left(n_2^2 - n_1^2\right)}$, as shown in Fig. 5. We verified the accuracy of the analytical estimate using numerical analysis. Specifically, we computed the m = 6 transmission minimum for w_s = 50, 75 and 100 nm using the Comsol RF solver. It should be noted that it was difficult to compute accurate minima for smaller values of w_s because of computational limitations. Note that there is excellent agreement between the analytical and numerical predictions as shown in Fig. 5. This result is significant because it implies that detectable shifts in the transmission spectrum can be achieved with the accumulation of nanoscale layers of biomaterial and little contrast in refractive index between the biomaterial and carrier fluid. We note that one of the important practical issues that will need to be addressed in further device optimization studies and in experimental realization of

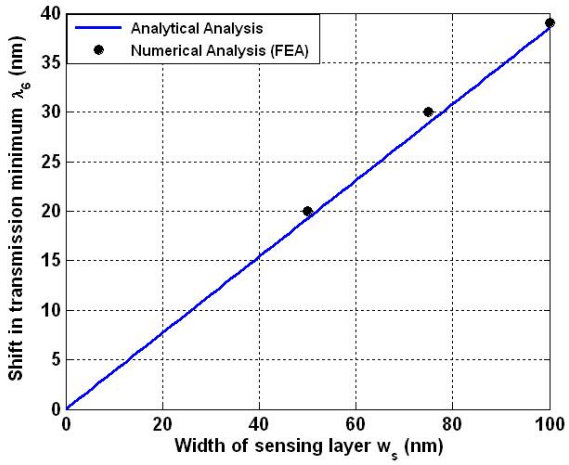

Fig. 5. Shift in transmission minima λ_6 versus width of sensing layer.

the proposed device is the effect of potentially nonuniform biomaterial accumulation that may affect the width of the transmission minimum and therefore, the FOM.

Finally, we consider the fluidic behavior of the sensor. Specifically, it is instructive to determine its operating pressure. To this end, we performed a three-dimensional computational fluid dynamic (CFD) analysis to determine the pressure required to fill the microchannels from an initial unfilled state. **We used the FLOW-3D commercial software for this analysis (www.flow3d.com), which is based on the volume of fluid VOF method.** Recall that the microchannels are 4 μm wide and that the substrate is 60 μm deep. The top and bottom feed channels are taken to be 12 μm high and the depth of the microchannels (into the page) is 40 μm. The carrier fluid is H_2O: viscosity η = 1x 10^{-6} m^2/s, density ρ = 1000 kg/m^3

and surface tension σ = 0.073 N/m. The CFD analysis indicates that a pressure of 2 Atm (30 psi) above ambient is sufficient to fill the sensor within 30 μs. A cross-sectional view of the CFD computational domain is shown Fig. 6a. The pressure distribution and velocity vectors in the fluid in this region at t = 30 μs is shown in Fig. 6b. The analysis was performed with 3 Atm of pressure applied at the top feed channels and 1Atm (ambient) pressure applied at the bottom feed channels.

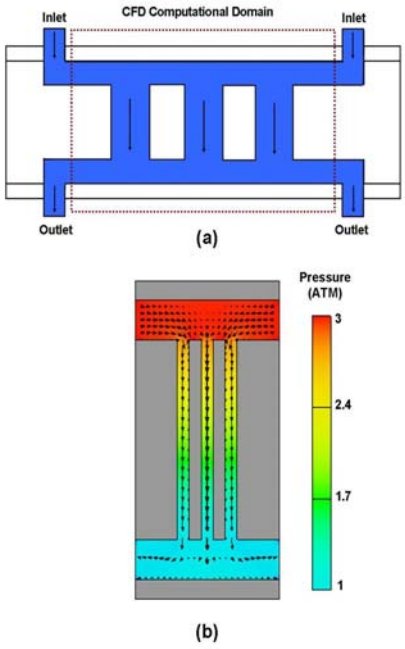

Fig. 6. CFD Analysis: (a) cross-sectional view of the CFD computational domain (enclosed in dotted line), (b) the pressure distribution and flow velocity vectors in the microchannels after 30 μs.

An important aspect of sensor performance that is related to the flow in the device involves the accumulation of biomaterial on the surfaces of the microchannels. This accumulation will be nonuniform and will vary from surface-to-surface when fluid is flowing through the device. Such nonuniformity and variation will degrade the sensitivity of the sensor. However, this can be overcome by operating the sensor in a quiescent fluidic mode wherein the biomaterial is introduced into the device under flow, but is allowed to accumulate on the walls of the microchannels under a no-flow condition. This would ensure a more uniform accumulation of biomaterial on each surface and less variation from surface-to-surface, which would produce a more well-defined optical signal as predicted above.

4. Conclusions

The field of optofluidics is its infancy and growing rapidly, especially for applications involving biosensing. Various sensor configurations have been proposed and analyzed.[13-16] In this paper, we have introduced a novel ARROW optofluidic biosensor and have studied its performance using 2D full-wave time-harmonic field analysis. Our results indicate that a detectable shift in transmission can be achieved with nanoscale layers of biomaterial and low contrast between the biomaterial and carrier fluid. The sensitivity of the studied proof-of-principle device is approximately 330 nm/RIU, which makes it competitive with a number of proposed sensor technologies (see Table 1 in ref. 15). The sensitivity can be optimized by varying different device parameters, notably the thickness of the substrate and the thickness and refractive index of the biolayer. The latter can be tuned by labeling the target biomolecules with a dielectric nanoparticle of a specified size and refractive index. An important feature of the sensor is that it can potentially function using focused illumination, without the need for fiber or waveguide coupled input/output signals. This feature enables 2D multiplexed operation, which is difficult to achieve using waveguide fed sensing elements. Furthermore, the sensor can be studied and optimized using analytical expressions that are based on 1D antiresonant waveguide model.

In this paper we addressed basic physical principles of the device operation, performed a detailed numerical characterization of the proposed device, and outlined the directions for further design optimization taking into account practical considerations, including losses

associated with leaky nature of ARROW structures, light confinement in the second lateral dimension, and the analysis of the effects of nonuniform biomaterial accumulation along the sensor length and across the channels that will be addressed in detail in future publications.

Acknowledgments

This work was partially supported by the US Air Force Office of Scientific Research, Award # FA95501010216.

References and links

[1] C. Monat, P. Domachuk and B. J. Eggleton, " Integrated optofluidics: A new river of light," Nature Photonics, 1, 106-114 (2007).

[2] D. Psaltis, S. R. Quake and C. H. Yang, " Developing optofluidic technology through the fusion of microfluidics and optics," Nature, 442, 381-386 (2006).

[3] H. Schmidt and A. R. Hawkins, " Optofluidic waveguides: I. Concepts and implementations," Microfluidics and Nanofluidics, 4(1-2), 3-16 (2008).

[4] F. Vollmer, D. Braun, A. Libchaber, M. Khoshsima, I. Teraoka, and S. Arnold, " Protein Detection by Optical Shift of a Resonant Microcavity," App. Phys. Lett., 80, 4057- 4059 (2002).

[5] A. Yalcin, K. C. Popat, O. C. Aldridge, T. A. Desai, J. Hryniewicz, N. Chbouki, B. E. Little, O. King, V. Van, S. Chu, D. Gill, M. Anthes-Washburn, M. S. Unlu, and B. B. Goldberg, "Optical Sensing of Biomolecules Using Microring Resonators," IEEE J. Sel. Top. Quantum Electron. 12, 148-155 (2006).

[6] A. M. Armani, R. P. Kulkarni, S. E. Fraser, R. C. Flagan, K. J. Vahala, "Label-Free, Single-Molecule Detection with Optical Microcavities," Science 317, 783 - 787 (2007).

[7] M. R. Lee and P. Fauchet, " Two-dimensional silicon photonic crystal based biosensing platform for protein detection," Opt. Express 15, 4530-4535 (2007)

[8] M.A. Duguay, Y. Kokobun and T.L. Koch, Antiresonant Reflecting Optical Waveguides in SiO2-Si multilayer structures, Appl. Phys. Lett. 49, 13-16 (1986).

[9] N. M. Litchinitser, A. K. Abeeluck, C. Headley, and B. J. Eggleton, " Antiresonant reflecting photonic crystal optical waveguides," Opt. Lett. 27, 1592 (2002).

[10] A. M. Zheltikov, " Ray-optic analysis of the (bio)sensing ability of ring-cladding hollow waveguides," Appl. Opt. 47, 3 474-479 (2008).

[11] N. M. Litchinitser, S. C. Dunn, P. E. Steinvurzel, B. J. Eggleton, T. P. White, R. C. McPhedran, and C. M. de Sterke, Application of an ARROW model for designing tunable photonic devices, Opt. Express 12, 1540-1550 (2004).

[12] N. M. Litchinitser and E. Poliakov, Antiresonant guiding microstructured optical fibers for sensing applications, Applied Physics B 81, Special Issue on Photonic Crystals, 347-351 (2005).

[13] T. Baba and Y. Kokubun, Dispersion and radiation loss characteristics of antiresonant reflecting optical waveguides; numerical results and analytical expressions, IEEE J. Quantum. Electron., Vol.28, pp. 1689-1700 (1992).

[14] J.L. Archambault, R.J. Balck, S. Lacroix, and J. Bures, Loss calculations for antiresonant Waveguides, J. Lightwave Technol., Vol.11, pp.416-423 (1993).

[15] I. M. White, and X. Fan, On the performance quantification of resonant refractive index sensors, Opt. Express 16(2), 1020-1028 (2008).

[16] J. Hu, X. Sun, A. Agarwal, and L. C. Kimerling, Design guidelines for optical resonator biochemical sensors, J. Opt. Soc. Am. B 26(5), 1032-1041 (2009).

[17] B. Lua, M. R. Smyth and R. O'Kennedy, Oriented Immobilization of Antibodies and Its Applications in lmmunoassays and Immunosensors, Analyst, **121**, 29R-32R (1996).

[18] X. Fang, V. K. S. Hsiao, V. P. Chodavarapu, A. H. Titus and A. N. Cartwright, Colorimetric Porous Photonic Bandgap Sensors with Integrated CMOS Color Detectors, IEEE Sensors Journal, 6 (3), 661-667 (2006).

[19] M. Svedendahl, S. Chen, A. Dmitriev, and M. Kall, Refractometric Sensing Using Propagating versus Localized Surface Plasmons: A Direct Comparison, Nano Lett. 9 (12), 4428-4433 (2009).